Int. J. Electrochem. Sci., 16 **(2021)** Article ID: 210563, doi: 10.20964/2021.05.47

International Journal of
ELECTROCHEMICAL
SCIENCE
www.electrochemsci.org

Electrodeposition of Ni-Co/Nano SiC Composites from a Citrate Bath and their Characterization

M. M. Kamel[1,*], *Q. Mohsen*[2], *Z. Abdel Hamid*[3], *S. M. Rashwan*[1], *I. S. Ibrahim*[4], *S. M. El–Sheikh*[3]

[1] Department of Chemistry, Faculty of Science, Suez Canal University, Ismailia 41522, Egypt.
[2] Department of Chemistry, College of Sciences, Taif University, Taif, Saudi Arabia.
[3] Central Metallurgical Research & Development Institute, Helwan, Cairo, Egypt.
[4] General Organization for Exports and Imports Control, Royal International Inspection Laboratories, Sokhna Port, Suez, Egypt.
[*]E-mail: medhat_darwish@science.suez.edu.eg

Received: 24 November 2020 / *Accepted:* 13 January 2021 / *Published:* 31 March 2021

The electrodeposition of Ni-Co/nano SiC composites onto steel substrates from a citrate bath was carried out under different experimental conditions. The addition of SiC to the bath increased the overvoltage for the Ni-Co alloy deposition. The morphology & structure of the deposits were checked by scanning microscope (SEM) & X-ray diffraction (XRD). The obtained composites were crystalline and had a face-centered cubic structure (FCC). The thickness of electrodeposited Ni-Co/ nano SiC composites gradually increases with increment the wt. % of SiC in the deposit. The corrosion resistance of composites, containing various amounts of SiC particles in 3.5 % NaCl solution, was predestined using linear polarization & impedance spectroscopy (EIS). As the percentage of SiC particles increases in the deposits, the corrosion resistance increases. Both microhardness and scratch resistances were ameliorated with increment the quantity of embedded SiC particles in the composites.

Keywords: Electrodeposition; Citrate bath; Ni-Co alloy; SiC nanoparticles; Composites

1. INTRODUCTION

Electrodeposited Ni-Co composite with excellent characteristics can be fabricated by the insertion of another-phase particles within the Ni-Co alloy matrix [1]. Therefore, it is reasonable to expect that electrodeposited Ni-Co/ceramic composite has high toughness & hardness. In addition to unique magnetic merits, good chemical resistance, and best corrosion resistance at higher temperatures than the normal Ni-Co alloy deposit. Actually, composites have the features of the electrodeposited alloy coating and the ceramic particles. Also, Ni-Co composite coatings have distinguished properties and applications than their corresponding Ni or Co composite coatings [1]. Ni-Co composites are foreseeable to be contributed in automotive and aerospace industrial areas. This is mainly due to their adequate attachment to the basis metal, minimal residual stress, great hardness, and corrosion resistance [2].

Various ceramic carbides such as SiC, WC, B_4C & Cr_3C_2, are co-deposited with metallic matrices to form composites. This is done where hardness & wear resistance & seal applications like jet engine seals, paper machine knives, and rubber-skiving knives, are the major requirements [3-15]. The most promising and famous metal carbide ceramic reinforcement is SiC particles. It possesses good mechanical resistance, excellent hardness &Young's modulus, great wear resistance and low cost [16]. For instance, Ni-Co/SiC nanocomposite coating matrix is used as a composite material in micro-devices [1].

For the Ni-Co alloy system, the standard reduction potentials of Ni & Co are - 0.25 & - 0.28 V, respectively. Therefore, nickel is preferentially deposited than cobalt. In order to facilitate satisfactory co-deposition of both metals, a complexing agent is added to the plating solution. The complexing agent either forms soluble complexes with both metals, or avoid the formation of insoluble compounds. Besides, it approaches the reduction potential of the two metals. It diminishes the activity of the nobler metallic ions in the plating bath, and hence, the closeness of the potentials of the metal ions can be achieved [17-19]. Citrate salts are the most hopeful complexing agents used in electrodeposited baths. Citrate anion is a poly-dentate carboxylic ligand with one hydroxyl group. It can form different complexes with a transition metal, in both acidic & basic solutions. In basic media, the dissociation of citric acid gives not only the three –COOH groups but also the hydroxyl group [20&21].

The advantages of citrate baths are not only their cheapness but also their non-polluting impact on the environment. Along the same lines, citrate anions are characterized by buffering, leveling, and brightening actions that permit the fabrication of high-quality coatings [22].

The target of this work is the electrodeposition of Ni-Co alloy coatings with SiC nanoparticles onto steel substrates from a citrate bath under different experimental conditions such as the quantity of SiC nanoparticles in the bath, deposition current, and bath temperature. Also, it aims to investigate the impact of these variables on the composition, appearance, and structure of the coatings. Furthermore, the variation of coating thickness, microhardness, and scratch-resistance of the coatings with the wt. % of SiC in the deposits was studied. Additionally, extensive studies on the corrosion resistance of Ni-Co alloys have distinct wt. % of SiC nanoparticles in 3.5 % NaCl are performed utilizing polarization and impedance (EIS) techniques.

2. EXPERIMENTAL

The SiC nanoparticles utilized in this treatise are pure (99.5 %) with particle size of 3-8 nm and obtained by the sol-gel method. Morphology and X-ray diffraction of the powder are checked utilizing transmission electron microscopy (TEM-1230, Japan) and X-ray diffractometer (X`pert Pro P analytical) as shown in Fig.1.

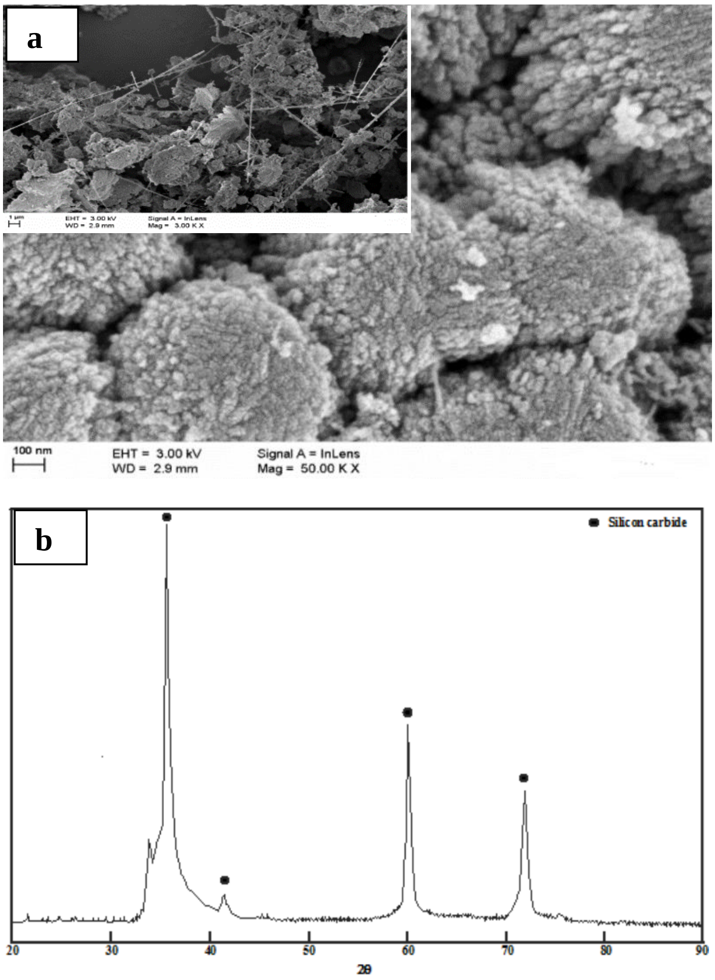

Figure 1. (a) TEM image and (b) XRD spectra of SiC nano-powder

Experimental work was accomplished from baths of composition: 0.08 M $NiSO_4.6H_2O$, 0.12 M $CoSO_4.7H_2O$, 0.20 M anhydrous Na_2SO_4 & 0.30 M $Na_3C_6H_5O_7.2H_2O$ and different amounts of SiC nano-sized powder. The pH was adjusted using NH_4OH or H_2SO_4 acid and measured by using Fisher pH-meter.

The practical system utilized was carried out in a cell made of a rectangular trough equipped with a steel coupon as a negative electrode (3 cm × 3 cm) and a stainless steel coupon (type – 304) as a positive electrode. The pretreatment proceedings of the cathode before the electroplating process were utilized to get a highly immaculate surface. Removing grease was done to tear out lubricating oil & greases from the cathode surface. The cathode was polished with different grades of polishing paper, washed with bi-distilled water, ethyl alcohol & weighed. The electrodeposition process was accomplished from a stirred solution. The deposition period was 20 minutes; thereafter the cathode substrate was taken, washed by bi- distilled water, dried & weighed. The content of SiC in the deposits was computed by EDX analysis.

Electrochemical corrosion of composites in 3.5 wt. % salt water (NaCl) solution was estimated by polarization measurements. This is accomplished with an electrochemical analyzer, supplied by IVIUM technologies, attached to a personal computer for potential monitoring & data procuration, and a conventional cell with a steel cathode with a surface area of 1 cm^2. All potentials measured versus saturated Hg_2Cl_2 electrode (SCE) with a Pt counter electrode. The polarization curves were swept from − 0.5 V, below OCP, to + 0.5 V at a scan rate of 0.5 mV s^{-1}. Three experiments were achieved for each sample to ensure the accuracy of the results.

EIS tests were established in a wide range of frequency 60 kHz - 10 MHz using a sine wave of 5 mV. 3.5 wt. % salt water solutions were utilized as a corrosive environment.

The surface morphology of composites was checked by SEM (QUANTA FEG 250) attached with energy dispersion spectrometer (EDX – FEI – QUANTA FEG 250) for the confirmation of the composition of the composites. The crystalline structure of the coatings was elucidated by X-ray diffractometer (X`pert Pro Panalytical), turn on at 35 kV and 40 mA with copper target radiation (λ = 0.154 nm). The thickness of the composite coatings was estimated by a thickness gauge (Model TT210). The microhardness was evaluated by a tester with a loading force of 100 grams for 5 seconds. The adherence of the deposited layer was established by the scratching test. For this test, 6 cuts were done on the examined sample by a cutting gadget with 6 cutting edges separated by 1 mm apart. Adhesion tape (AME Ricav Tape) was promptly utilized to the cutting area and thereafter taken away quickly by withdrawing at right angles to the examined sample. Referring to national standards ISO 2409, the coating was categorized into 6 types.

3. RESULTS AND DISCUSSION

3.1. Polarization tests

Polarization measurements were carried out to examine the impact of SiC nanoparticles on the deposition of the Ni-Co alloy [23 & 24]. Polarization experiments involve changing the working electrode potential and recording the output current [24 -26].

The influence of increasing the amount of SiC nanoparticles in the deposition bath on the cathodic polarization of Ni-Co alloy is demonstrated in Fig.2. Increment the particle concentration causes the polarization curves to shift towards the more negative magnitudes. This behavior is ascribed to the adsorption of SiC particles at the surface of the cathode. This causes surface blockage and reducing the active surface area of cathode available for metal reduction [27].

Wu and others [28] reported that the required energy for depositing cations, which are solvated with water and adsorbed on the ceramic particle surface is greater than the energy for the free solvated metal cations. Thence, the deposition potential shifts toward high negative magnitudes as the amount of SiC increases in the plating solution. Additionally, such a shift towards higher reduction potentials can be correlated to the deficiency in the ionic transfer by the inert particles.

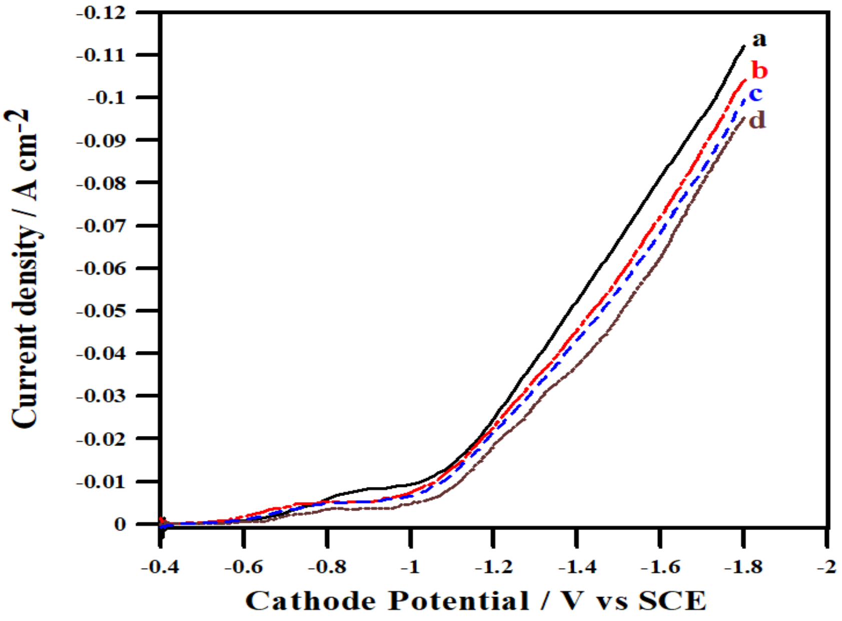

Figure 2. Polarization curves for the deposition of Ni-Co/ nano SiC composite on steel substrate at pH 10, temperature 25 °C and stirring speed 600 rpm from solutions comprising 0.08 M $NiSO_4$. $6H_2O$, 0.12 M $CoSO_4$. $7H_2O$, 0.3 M $Na_3C_6H_5O_7$. $2H_2O$, 0.2 M Na_2SO_4 and different amounts of nano-sized SiC: (a) 0, (b) 2, (c) 3.5 & (d) 5 g/L. Scan rate = 20 mV/s

3.2 Composition of the deposits

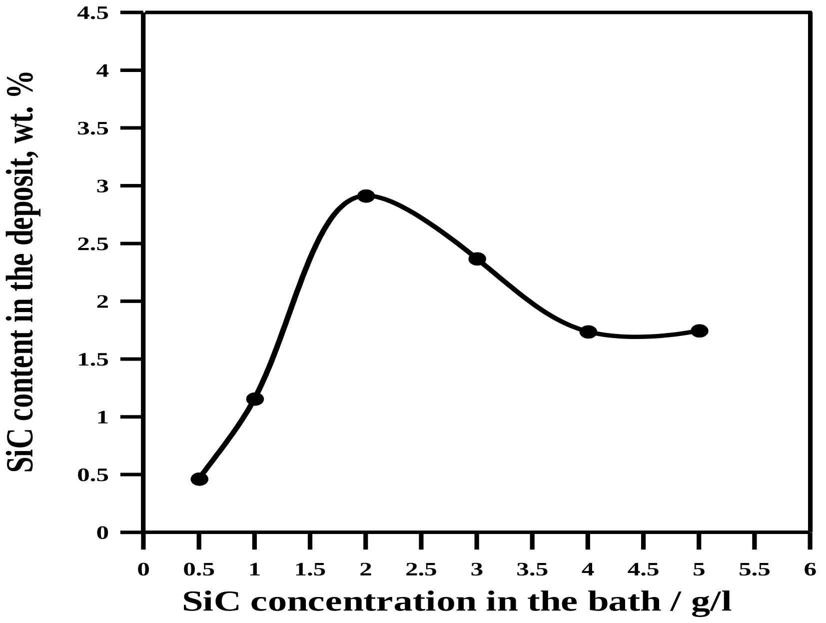

Figure 3. Impact of nano-sized SiC amount in the bath on the SiC % in the Ni-Co/SiC composite

The particle amount and their dispensation in electrodeposited composites rely on many correlated factors [29] like concentration and size of suspended particles, the deposition current, deposition temperature, pH, agitation, and time. The impacts of some of these variables on the deposition process have been discussed. Broadly, the amount of embedded particles in the composite relies on their quantity in the bath [30]. It has been acknowledged [31] that a large quantity of solid particles in the bath, leads to a high weight % of the ceramic particles in the composite. Fig.3 illustrates the impact of SiC quantity in the bath on their wt. % in the deposit. SiC content gradually increases with increasing its amount in the bath till attain the utmost value at concentration 2 g/L and then after decreases.

This behavior can be discussed by Guglielmi's model [32]. Guglielmi concluded that: as the quantity of the particles increases in the bath, the number of particles traveled from the electrolyte bulk to the cathode surface is increased. This will enhance the possibility of adsorption at the substrate surface and increment the quantity of the co-deposited SiC particles. However, the limited content could be attributed to steady-state equilibrium. At this point, the number of co-deposited solid particles is equal that attaining the cathode surface. At concentrations higher than the optimum one, solid particles tend to coalesce in the bath and therefore, the particle insertion in the deposited matrix decreases [33 – 37].

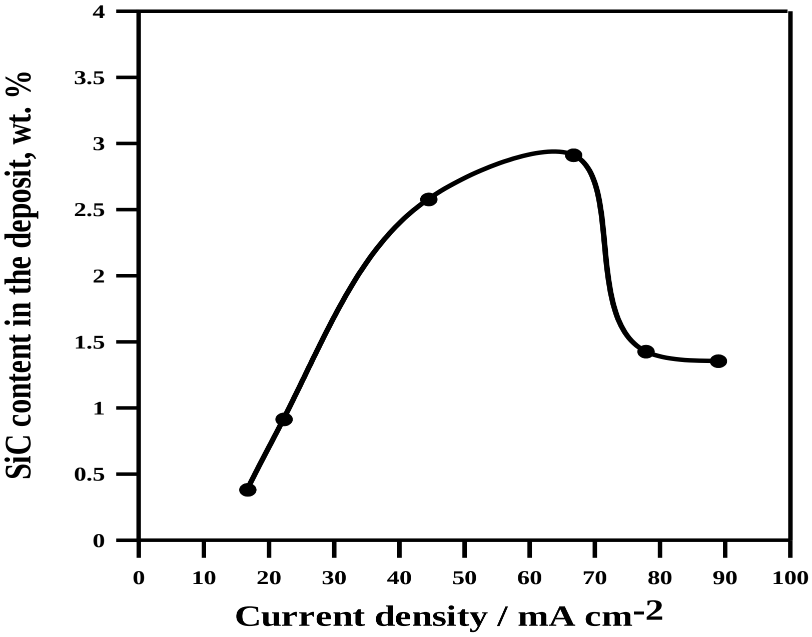

Figure 4. Impact of applied current density on the SiC % in the Ni-Co/SiC composite

Current density is the crucial agent that impacts the insertion of particles into a metallic matrix [38]. Fig. 4 displays the impact of the imposed current density on the wt. % of SiC nanoparticles in composite. The dual role of current density in particle dispersal & deposition may be argued via the competition between the insertion rate of inert particles & the rate of discharge of metallic cations [39]. For small current densities, the metal ions (Ni^{2+} and Co^{2+}) diffuse slowly, and a fewer number of ions get adsorbed on the SiC nanoparticles. As a result, the concentration of metallic ions and ions that adsorbed on the inert SiC nanoparticles diminished, resulting in a slow metal deposition rate. Furthermore, the force of Coulomb between adsorbed ions on the particles and the cathode may be slight. This gives rise to a part of particles that attain the cathode surface, to be moved away because of agitation. Therefore, a small content of the co-deposited SiC nanoparticles is obtained [40 & 41].

Moreover, because of differences in the amounts of activation energy required for deposition; the free metal ions ask little energy for deposition. Consequently, the free Ni^{2+} and Co^{2+} ions will be deposited at the cathode surface rather than the SiC nanoparticles. This will minimize the particle concentration in the composite.

As the current growing, the difference in activation energy decreases and becomes less important because there is enough energy to promote the diffusion and convection of the particles. Accordingly, the electrolyte at the vicinity of the cathode surface becomes free of metallic ions. Also, polarization and deposition rate increase, leading to an enhancement in the deposition of both metallic ions and the inert particles [42 – 45]. Furthermore, the growth of metal crystallites is adequate to encapsulate the SiC nanoparticles at the confined time interval for which they lodging at the surface of the substrate. This leads to a greater contribution of SiC nanoparticles in the composites [41].

The energy required to deposit the solvated and adsorbed Ni^{2+} and Co^{2+} ions at the surface of silicon carbide nanoparticles, is higher than that for the free Ni^{2+} and Co^{2+} ions [46]. As a result, the diffusion of Ni^{2+} and Co^{2+} ions towards the cathode is more rapid than adsorbed particles (Ni-SiC & Co-SiC). This will cause rapid reduction of metal ions and decreases the quantity of SiC nanoparticles in the composites [47]. Notwithstanding, the appearance of H_2 bubbles at high current densities causes a decay in the current efficacy and handicaps the attachment of SiC at the metal ions surfaces.

Figure 5 depicts the impact of bath temperature on the wt. % of SiC nanoparticles in Ni-Co alloy. The wt. % of SiC increases with increasing bath temperature up to 25 ° C. Increasing temperature enhances the co-deposition of SiC nanoparticles as it increases the kinetic activity of the particles. As the temperature rises, the transfer of metal ions is highly improved, which results in an increment of the deposition rate and the kinetic energy of the particles. Langmuir reported that increasing bath temperature decreases the adsorbability of the particles and thus makes it more strenuous for SiC particles to be contained in the composite. This will decrease the wt. % of the SiC particles in the coating [48]. Moreover, the maxima observed for the temperature impact could be assigned to the transition from activation to diffusion-controlled reaction [45].

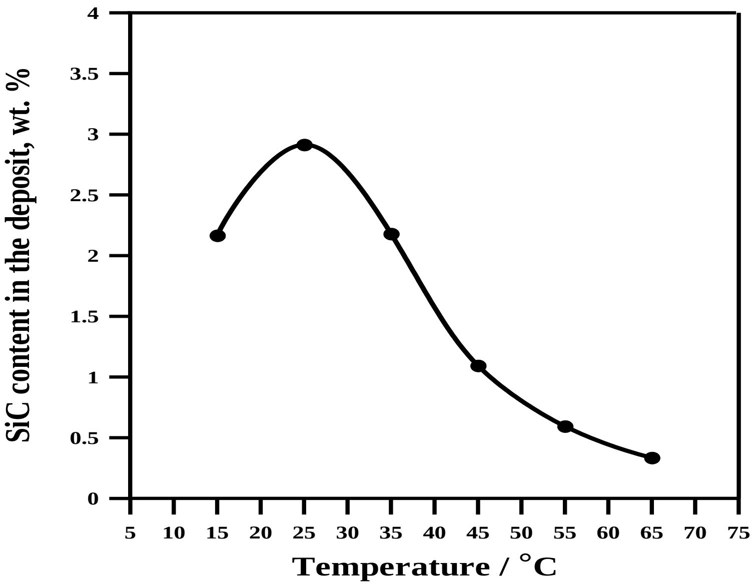

Figure 5. Effect of bath temperature on the SiC % in the Ni-Co/SiC composite

3.3 Appearance and structure of the deposits

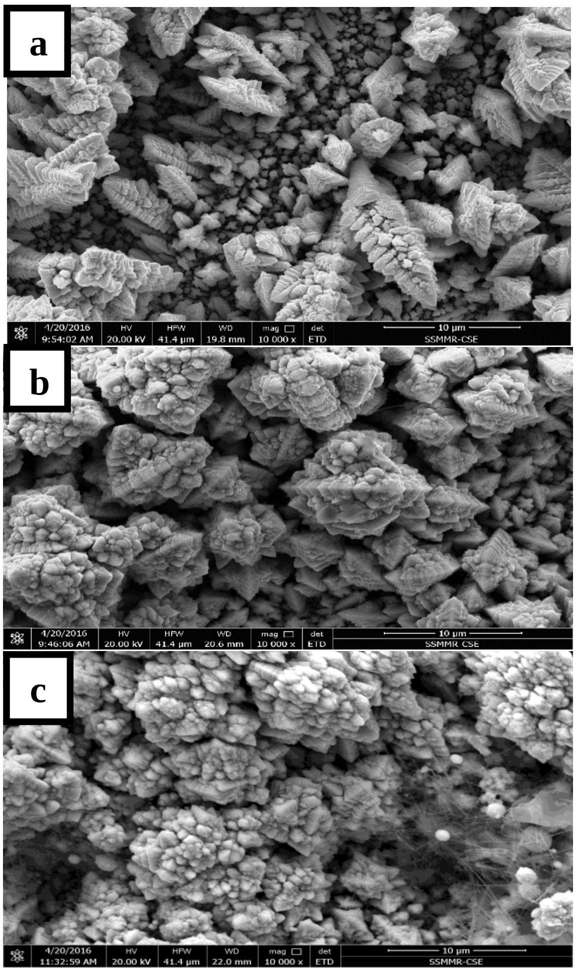

Figure 6. SEM morphology of electrodeposited Ni-Co alloy containing: (a) 0, (b) 0.46 and (c) 1.74 wt. % nano-sized SiC

Surface examination of the electrodeposits obtained under different experimental conditions investigated by scanning microscopy. All the electrodeposited Ni-Co composite coatings are regular compact and have a dull dark gray color. The darkness of the electrodeposited composites increases with raising the particle amount in the bath. Fig. 6 demonstrates the impact of increasing nanosized SiC amount in the deposit on the morphology of electrodeposited Ni-Co composites. The free-deposited alloy is dense and compact. The surface contains some holes corresponding to hydrogen evolution bubbles.

It is worth observing some dendrites that are randomly distributed over the cathode surface, Fig. 6a. The addition of 0.5 g/L SiC particles to the plating bath results in the disappearance of the dendrites and causes a reduction in the size of the electrodeposits, Fig. 6b. Further addition of SiC up to 2g/L changed the morphology of electrodeposited composites and causes more grain size refinement, Fig.6c. This modification of the structure may be attributed to an increment in the polarization that facilitates the rate of nucleation & favors the formation of fine-grained deposits.

The minimizing in the crystal size of the Ni-Co matrix is attributed to the adding of inert particles to the plating bath. During the growth of the electrodeposited coating, there is a rivalry between the formation of new nuclei & the growth of the existing nuclei. The inert particles attached to the growing crystal, suppress its further growth, and provide more nucleation sites. i.e., they increase the nucleation sites for the reduction of metal ions and nucleation of metal grains. This effect controls and delays the crystal growth [43, 48 & 49].

The phase composition & crystal structure of Ni-Co composites containing different wt. % of SiC nanoparticles were examined using X-Ray diffraction measurements. The impact of particle amount in the deposit on XRD spectra of electroplated Ni-Co/ SiC nanocomposites is recognized in Fig.7. The structure of the electrodeposited composites is a solid solution of nickel and cobalt with a face-centered cubic (FCC) phase [24]. The electrodeposited alloys exhibit three well-defined diffraction peaks located at around 44.5°, 51.8°, and 76.4. These peaks are assigned to (111), (200), and (220) growth orientation planes, respectively [50 &51]. They are sharp, indicating a good crystalline structure. The intensity of the (111) peak is the strongest one. The peaks corresponding to the SiC nanoparticles phase are not found in the spectra due to its small size (3-8 nm) and lower content in the deposit. Their existence in the deposits is detected and confirmed by EDX analysis, Fig. 8. The intensity of the plane slightly diminishes as the SiC amount increases in the deposit.

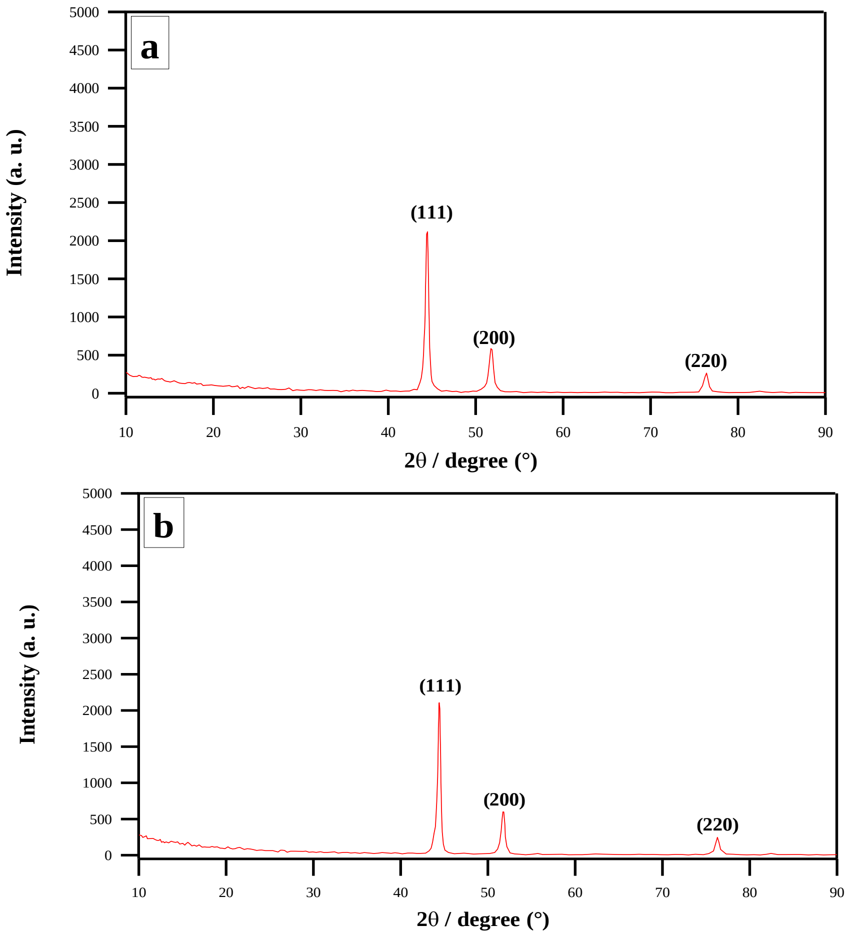

Figure7. XRD spectra of electrodeposited Ni-Co alloy containing: (a) 0 and (b) 1.74 wt. % nano-sized SiC

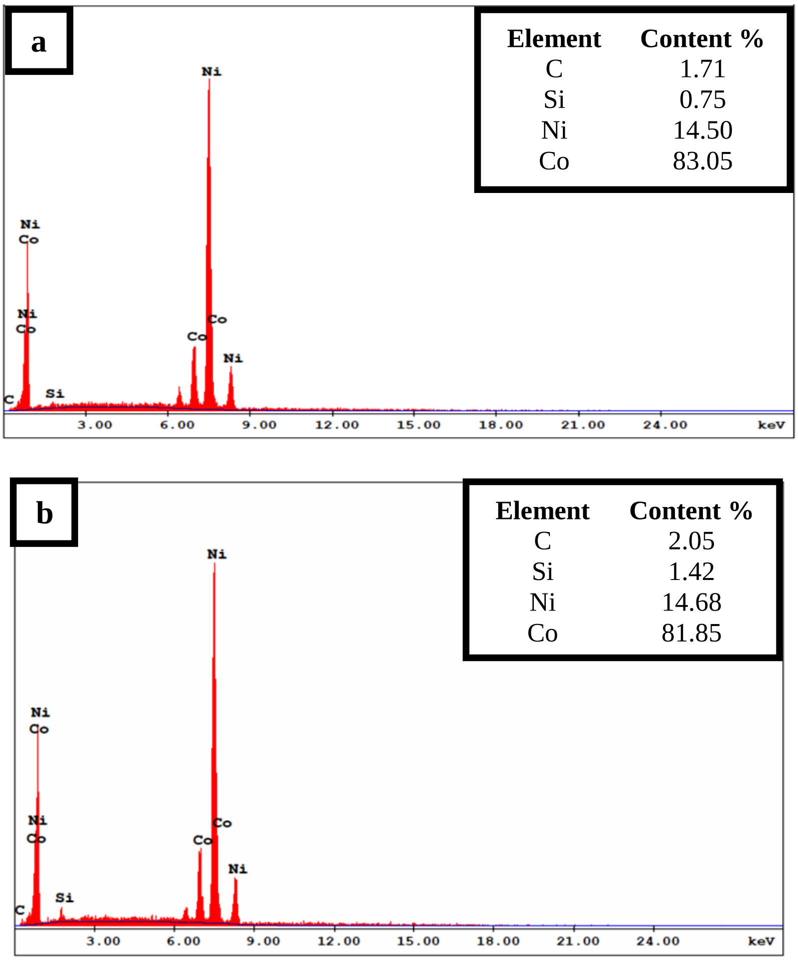

Element	**Content %**
C	1.71
Si	0.75
Ni	14.50
Co	83.05

Element	**Content %**
C	2.05
Si	1.42
Ni	14.68
Co	81.85

Figure 8. EDX analysis patterns of electrodeposited Ni-Co alloy containing: (a) 0.46 and (b) 2.9 wt. % nano-sized SiC

3.4 Coating thickness

The thickness of electrodeposits depends on the electrodeposition parameters during the deposition process, e.g. the applied current and the electrolysis period. Also, the quantity of the dispersed particles in the bath impacts the coating thickness [52].

Figure 9 displays the variation of the thickness of electrodeposited Ni-Co composites coating with the amount of incorporated SiC particles. The thickness slightly decreases with increment the particles content in the deposits. The incorporated SiC particles act as an inhibitor for grain growth and enable nucleation sites for the growth of fresh grains. Therefore, thin composite coatings are produced. Moreover, the evolution of hydrogen gas at the cathode can also diminish the thickness of the coating [53].

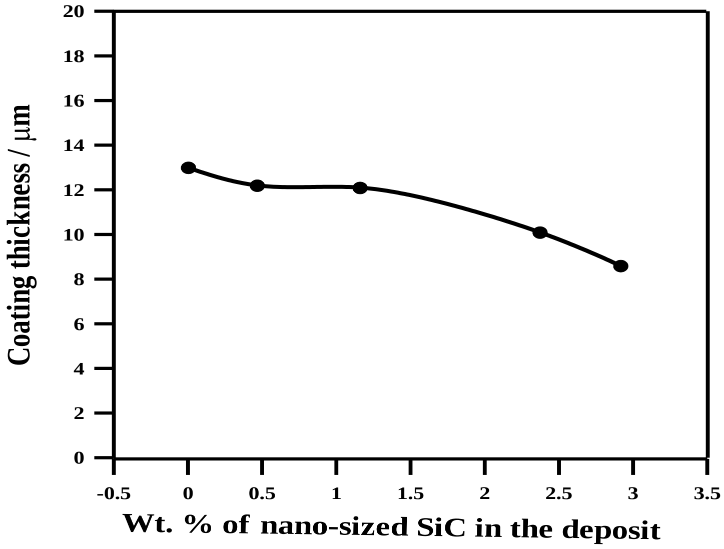

Figure 9. Variation of Ni-Co composite thickness with the amount of incorporated nano-sized SiC

3.5 Electrochemical investigation

3.5.1 Tafel study

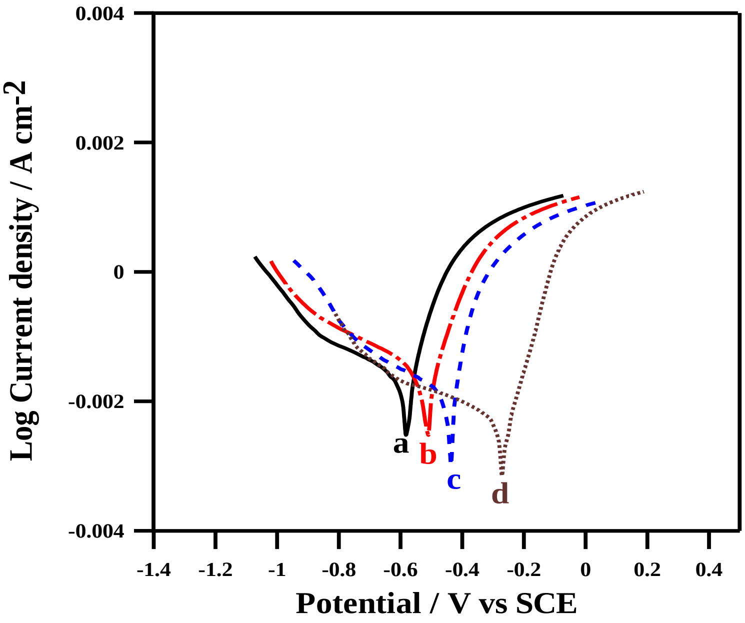

Figure 10. Potentiodynamic polarization curves for Ni-Co/ nano SiC composite containing different amounts of nano-sized SiC: (a) 0, (b) 0.46, (c) 1.74 & (d) 2.9 wt. % in 3.5 % salt water

Figure 10 displays the potentiodynamic polarization curves for Ni-Co composite coatings have varying amounts of SiC nanoparticles in 3.5 % salt water solution. The existence of inert particles in the metallic coating affects the kinetics of anodic & cathodic reactions [23]. For the cathodic reaction, the addition of inert particles causes some retardation for the hydrogen gas evolution. In the anodic reaction, the adsorption of inert particles on the electrode surface reduces its active surface area. The magnitudes of β_a & β_c, for nano-composites are unlike the pure Ni-Co alloy coating, Table (1). This is because of the amendments at the coating surface, induced by the inert particle co-deposition [54& 55].

Table 1. Corrosion parameters obtained from Tafel plots of the plain Ni-Co alloy & Ni-Co/ nano SiC composites comprising variant wt. % of nano-sized SiC.

Sample	$\beta_a \times 10^{-3}$ (V/dec)	$\beta_c \times 10^{-3}$ (V/dec)	$I_{corr} \times 10^{-3}$ (A/cm^2)	R_p (Ω)	$E_{corr} \times 10^{-3}$ (V/ SCE)	CR (mpy)
Ni-Co + 0 wt. % SiC	110	-45	27	508	-775	3.67×10^{-4}
Ni-Co + 0.46 wt. % SiC	29	-130	22	461	-715	3.05×10^{-4}
Ni-Co + 1.74 wt. % SiC	20	-63	2	2643	-568	3.35×10^{-5}
Ni-Co + 2.91 wt. % SiC	95	-32	1	10494	-324	1.33×10^{-5}

The data of Table (1) demonstrate that increasing SiC nanoparticle amount in the composite tends to decrease the I_{corr} & shifts the E_{corr} towards noble potentials. The polarization resistance (R_p), which is utilized to assess the resistance of the metal under consideration against corrosion, increases with particle content and hence, the corrosion rate (CR) decreases. There is no question that Ni-Co composite coating containing SiC in a nano-size possesses superior corrosion resistance than pure Ni-Co coating [56 - 58].

The role of SiC ceramic nanoparticles in improving the corrosion resistance of Ni-Co composites can be assigned to the following causes:

- The inert particles behave as physical barrier to the inception and the enhancement of corrosion. They amend the fine-structure of the metallic coating by filling in or occupying some structural blemishes like crevices, cracks, voids, and porosities. The dimension of these blemishes is in submicron and micron ranges.
- The existence of SiC inert particles in the Ni-Co lattice reduces its efficient surface area exposed to the corrosive solution, resulting in improved corrosion resistance. Furthermore, these inert particles participate in the passivation process of the Ni-Co alloy [59].
- The size and the allocation of SiC particles in the deposited layer play a substantial role in the enhancement of the corrosion resistance of Ni-Co composite. Uniform particle distribution enhances the properties of metallic coatings [54 & 60].

3.5.2. Impedance measurements

EIS is a unique tool for investigating the coating disintegration and corrosion protection of distinct coatings [21]. The EIS data are represented by Nyquist or Bode plots.

For Bode plots, the disintegration rate can be evaluated with the help of the impedance modulus (Z_{mod}). The high magnitude of Z_{mod} indicates a low dissolution rate for the coating. As the percentage of SiC nanoparticles in the deposit increases, the dissolution resistance increases, Fig. 11. Straightforward Randles circuit, Fig. (12), is used to fit the graphs obtained for the investigated composites [61 & 62]. The fitted values are collected in Table (2). For the investigated circuit, the charge transfer resistance R_{ct} is parallel connected to the double-layer capacitance C_{dl}. The output of both is connected in series to the solution resistance R_s. Our experimental results are fully consistent with this model. CPE_{dl} is the non-perfect double-layer capacitance. The constant phase element (CPE), which permits for the impacts of deflection to ideality, is utilized rather than the electric double-layer capacitance (C_{dl}). It provides a more precise fitting to the impedance demeanor of the electrical double-layer. It resembles a capacitor, but the phase angle does not equal 90°. The CPE is commonly applied to expound the non-homogeneous system because of the coarseness, porosity, & heterogeneity of the electrode surface [62]. The double-layer capacitance enables acquaintance on the polarity and the quantity of charge at the coating/electrolyte boundary [61]. The existence of an electrical double-layer at the electrode/electrolyte boundary elucidates that the corrosion process is dominance by the charge-transfer process [42].

The big magnitudes of R_{ct} and small magnitudes of CPE_{dl} glimpse a better corrosion defense potency of the coatings. The low (CPE) values confirmed that the coatings are relatively homogenous, less porous, and less rough [62]. An analogous proclivity has been remarked also with the R_p magnitudes assuring the reality that the corrosion resistance of Ni-Co alloy depends on the intromission of SiC nanoparticles. The insertion of SiC into the alloy matrix can plug some of the voids in the matrix and prohibit the diffusion of corrosive solution containing Cl^- ions along the boundary.

Furthermore, the existence of SiC in the conductive Ni-Co alloy could stop the transfer of the electrical current, as the SiC particles can be presumed to be idealistic insulators. Also, the intercalation of SiC nanoparticles minimizes the apparent area exposed to corrosion giving rise to larger values of R_{ct} and smaller values of CPE_{dl} for Ni-Co/ SiC nano-composites than pure Ni-Co alloy [21].

Fig. 13 illustrates the Nyquist diagrams for the coated steel with plain Ni-Co alloy and Ni-Co/SiC nanoparticles composites containing variant quantities of SiC nanoparticles. The diagram comprises a capacitive single semi-circle noose, which is correlated to the electrochemical arranging between the R_{ct}, and the CPE_{dl}. This capacitive noose can be explicated as the CPE_{dl} is parallel to the R_{ct} [47, 48 & 63]. Over and above, the apparition of only a singular semi-circle referred that deposit/solution boundaries manifest charge-transfer behavior. Besides, the disintegration process of the composites comprises a single-time constant ($\tau = R_{ct}\ CPE_{dl}$) referring to the presence of a double-layer at composite/electrolyte boundary [48 & 61].

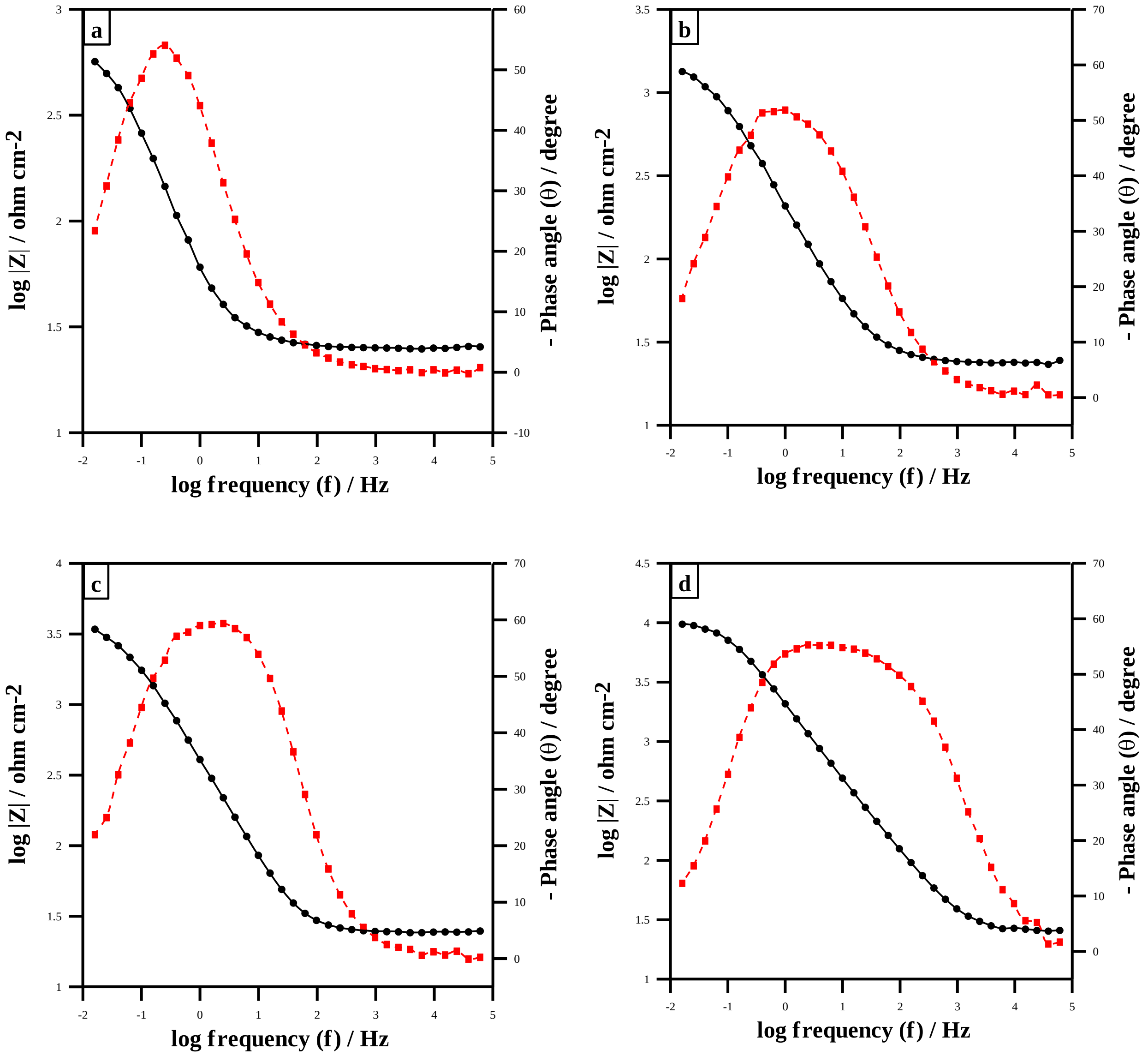

Figure 11. Bode and phase angle plots of impedance spectrum for electrodeposited Ni-Co composite coatings comprising (a) 0, (b) 0.46 (c) 1.74 & (d) 2.9 wt. % of nano-sized SiC in 3.5 % NaCl.

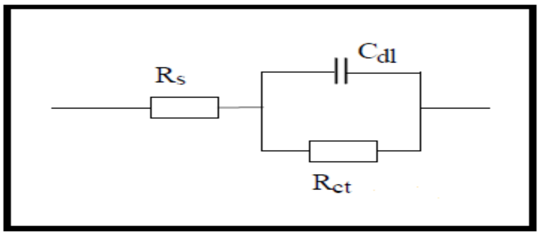

Figure 12. Equivalent circuit diagram for impedance spectra of electrodeposited Ni-Co composite coatings comprising variant quantities of nano-sized SiC in 3.5 % NaCl

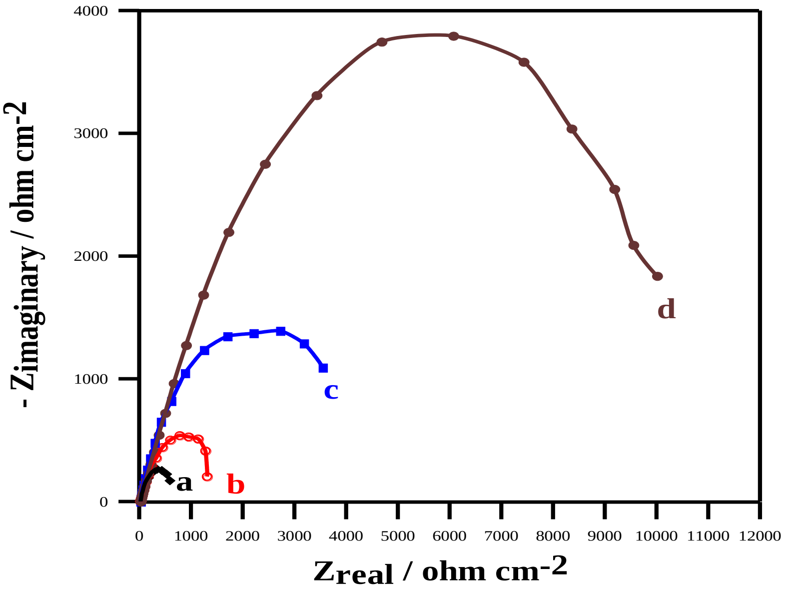

Figure 13. Nyquist plots for electrodeosited Ni-Co composite coatings comprising (a) 0, (b) 0.46 (c) 1.74 and (d) 2.9 wt. % of nano-sized SiC in 3.5 % salt water.

The Nyquist diagram, Fig. 13, for pure alloy & Ni-Co/ SiC nanocomposite coatings are like in shape but differ highly in their diameter size. This proves that the dissolution process in both cases follows the same mechanism. The width of the semicircle determines the corrosion resistance of the coatings, and the larger width indicates the higher corrosion resistance. The impedance variables deduced from the Nyquist diagram are illustrated in Table 2. The R_{ct} magnitudes were increased, whereas CPE values decreased by introducing more of the quantity of SiC nanoparticles in the solution. The diminishing in the CPE magnitudes is assigned to the attachment of SiC nanoparticles with the coating. The results reported from EIS studies are in good coincidence with those of potentiodynamic polarization studies.

Table 2. Electrochemical parameters of EIS measurements of the plain Ni-Co alloy & Ni-Co/ nano SiC composites with various wt. % of nano-sized SiC.

Sample	**R_s (ohm cm^2)**	**R_{ct} (ohm cm^2)**	**CPE_{dl} (F/ cm^2)**
Ni-Co + 0 wt. % SiC	33.8	572	6.49×10^{-3}
Ni-Co + 0.46 wt. % SiC	57.2	1247	1.64×10^{-3}
Ni-Co + 1.74 wt. % SiC	99.8	3357	8.24×10^{-4}
Ni-Co + 2.91 wt. % SiC	300	9185	1.24×10^{-4}

3.6 Microhardness

The mechanical characteristics of metal-matrix composites rely on several agents: (i) The particle type, (ii) The number of particles, (iii) The sparse phase's size, (iv)The inter-particle wideness,

(v) The particles allocation, (vi) The shape of the particles, (vii) The texture and mechanical features of the matrix & particles boundaries [64].

The data of Fig. 14 demonstrate that the microhardness of Ni-Co/ nano SiC composite linearly increases with the quantity of embedded SiC nanoparticles in the coatings. This marked increase in microhardness may ascribe to particle-strengthening, dispersion strengthening, or grain refinement strengthening [65]. The first has an insignificant influence on increasing microhardness because the size of nano-sized SiC particles is lower than 1 µm. Dispersion-strengthening correlated with the coalition of small particles with a size ranging from 0.01 to 1µm and volume fraction < 15 % through a dislocation-particle interaction. This factor has a significant impact on increasing microhardness because the size of SiC particles is smaller than 1 µm. For this mechanism, the matrix totes the load, and the small particles hinder/obstruct the dislocation movement of the metallic matrix. Also, they suppress the matrix disfigurement by a nano-mechanical constraint, and accordingly, toughness is achieved.

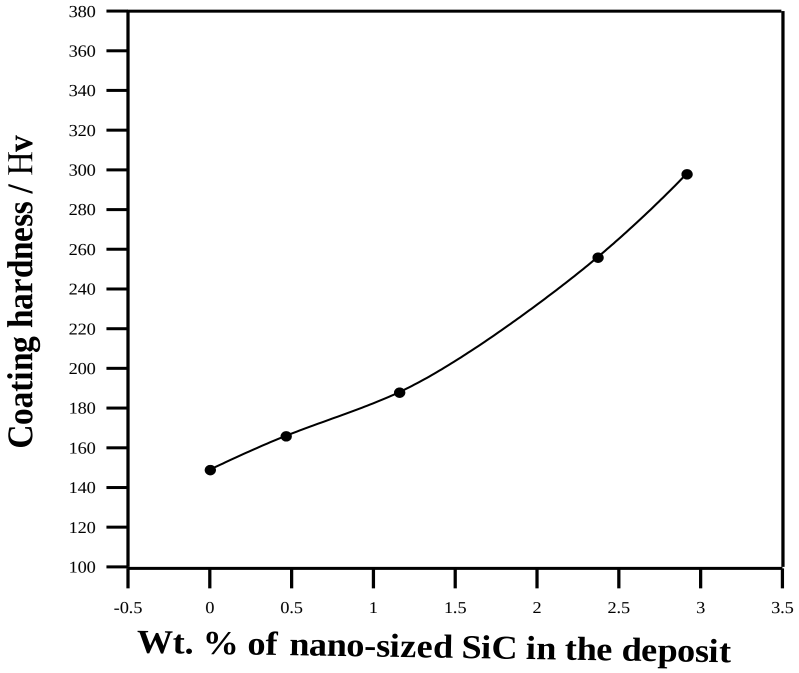

Figure 14. Microhardness of Ni-Co composite containing different amounts of nano-sized SiC.

The dispersive strengthening effect becomes stronger with increment the quantity of inert particles in the coating and therefore, the microhardness of composite increases. Similar trends were proclaimed with other particles in the nickel composite [64 & 65]. Grain refinement strengthening is linked to the formation of fine-nuclei at the surface of the inert particles, leading to a comprehensive structural refinement. The existence of nanoparticles in the metal matrix impacts the competitive formation of metal nuclei & crystal growth, randomness of the even structure and so, the texture of the metal matrix turns into fine crystals. Accordingly, a uniform surface with a small crystal size is acquired and the microhardness increases as a result [49, 37].

Furthermore, a portion of the microhardness promotion in the Ni-Co coatings containing SiC nanoparticles is correlated to the great microhardness of the Ni-Co matrix, because of the formation of substitution solid solutions. The solid solutions increment the microhardness of coatings via a solid solution-hardening mechanism [54 & 56].

3.7 Adhesion property

The adhesion performance between the deposited film & the steel substrate was investigated by the scratch test. A high adhesive Ni-Co/SiC nanocomposite layer with steel substrate was found. It is obvious that the films still adhered well to the substrate showing a good adherence between the Ni-Co/SiC film & the steel substrate. This reflects the good plating quality without swelling and peeling off. Moreover, the adhesion force is great for the deposited layers containing different wt. % of SiC.

In comparison to the standard results, the edges of the cuts are smooth and none of the squares of the lattice is detached. These results comply with the (0) degree according to ISO 2409 classification as depicted in Fig. (15).

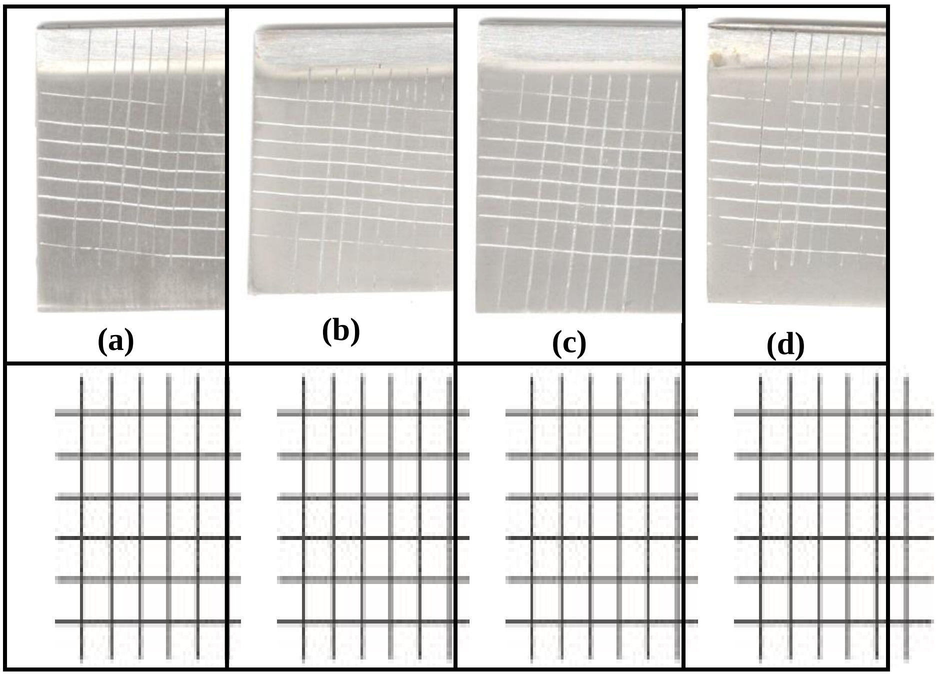

Figure 15. Adhesion of Ni-Co/ nano SiC composite coatings with different quantities of SiC: (a) 0, (b) 0.46 (c) 1.74 & (d) 2.9 wt. % of nano-sized SiC.

4. CONCLUSIONS

SiC nanoparticles were co-deposited with Ni-Co alloy using the electrodeposition technique. The deposition is carried out from a citrate bath. The effect of plating parameters like SiC amount in the plating bath, temperature, and depositing current on the wt. % of SiC in the deposit was investigated. The wt. % of SiC nanoparticles in the composites increases with the amount of the ceramic particles in the bath, the deposition current, and decreasing deposition temperature. The presence of SiC nanoparticles in the plating bath increases the cathodic polarization for alloy electrodeposition. The coating thickness of the Ni-Co matrix diminishes by increment the quantity of embedded nanosized SiC. The addition of SiC nanoparticles to Ni-Co coatings enhances the corrosion resistance. It also ameliorates the microhardness and the adhesion force between the coating film and steel substrate.

ACKNOWLEDGMENTS
Taif University Researchers supporting project number (TURSP – 2020/19), Taif University, Taif, Saudi Arabia.

References

1. L. Shi, C. Sun, P. Gao, F. Zhou and W. Liu, *Appl. Surf. Sci*., 252 (2006) 3591.
2. S. M. Lari Baghal, A. Amadeh, M. Heydarzadeh Sohi and S. M. M. Hadavi, *Mater. Sci. Eng*. A, 559 (2013) 583.
3. A. Abdel Aal, Z. I. Zaki and Z. Abdel Hamid, *Mater. Sci. Eng*., A, 447 (2007) 87.
4. H. Ben Temam, A. Chala and S. Rahmane, *Surf. Coat. Technol*., 205 (2011) S161.
5. E. Rudnik, L. Burzyńska and M. Gut, *Mater. Chem. Phys*., 126 (2011) 573.
6. G. Sharma, R. K. Yadava and V. K. Sharma, *Bull. Mater. Sci*., 29 (5) (2006) 491.
7. W. Cui, K. Wang, F. Xia and P. Wang, *Ceram. Int*., 44 (5) (2018) 5500.
8. A. Lanzutti, M. Lekka, C. de Leitenburg and L. Fedrizzi, *Tribol. Int*., 132, (2019) 50.
9. P. Jenczyk, M. Gawrońska, W. Dera, J. Chrzanowska-Giżyńska, P. Denis and D. M. Jarząbek, *Ceram. Int., 45 (17) Part* B, (2019) 23540.
10. C. Ma, D. Zhao and Z. Ma, *Ceram. Int., 46 (8) Part* B, (2020) 12128.
11. C. Ma, D. Zhao, W. Liu, F. Xia, P. Jin and C. Sun, *Ceram. Int.,* 46 (11) Part A, (2020) 17631.
12. N. P. Wasekar, L. Bathini, L. Ramakrishna, D. S Rao and G. Padmanabham, *Appl. Surf. Sci.,* 527 (2020) 146896.
13. W. Jiang, L. Shen, M. Xu, Z. Wang and Z. Tian *J. Alloys Compd*., 791 (2019) 847.
14. P. Jin, C. Sun, C. Zhou, L. Shi and C. Liu, *Ceram. Int*., 45, (16) (2019) 20155.
15. B. Li and W. Zhang, *Ultrason Sonochem*., 61 (2020) 104837.
16. Z. Wu, B. Shen and L. Liu, *Surf. Coat. Technol*., 206 (2012) 3173.
17. Y. Yang and Y. F. Cheng, *Surf. Coat. Technol*., 205 (2011) 3198.
18. B. Bakhit, A. Akbari, F. Nasirpouri and M. G. Hosseini, *Appl. Surf. Sci*., 307 (2014) 351.
19. O. Gylienė and J. Aikaitė, *J. Hazard. Mater*., B109 (2004) 105.
20. E. Beltowska–Lehman and P. Indyka, *Thin Solid Films*, 520 (2012) 2046.
21. L. Trinta de Farias, A. S. Luna, D. C. Baptista do Lago and L. Ferreira de Senna, *Mater. Res*., 11 (1) (2008) 1.
22. M. M. Kamel, Z. M. Anwer, I. T. Abdel–Salam and I. S. Ibrahim, *Trans. Inst. Met. Finish*., 88 (4) (2010) 191.
23. S. Özkan, G.Hapçı, G. Orhan and K. Kazmanlı, *Surf. Coat. Technol*., 232 (2013) 734.
24. M. M. Kamel, Z. Abdel Hamid, S. M. Rashwan, I. S. Ibrahim, S. M. El-Sheikh and M. M. Mohamed*, Int. J. Electrochem. Sci*., 15 (2020) 6343.
25. V. Zarghami and M. Ghorbani, *J. Alloys Compd*., 598 (2014) 236.
26. K. Vathsala and T. V. Venkatesha, *Appl. Surf. Sci*., 257 (2011) 8929.

27. Alina–Crina Ciubotariu, L. Benea, M. Lakatos–Varsanyi and V. Dragan, *Electrochim. Acta*, 53 (2008) 4557.
28. G. Wu, N. Li, D. Zhou and K. Mitsuo, *Surf. Coat. Technol.,* 176 (2004) 157.
29. L. Tian and J. Xu, *Appl. Surf. Sci.,* 257 (2011) 7615.
30. H. Gül, M. Uysal, H. Akbulut and A. Alp, *Surf. Coat. Technol*., 258 (2014) 1202.
31. C. T. J. Low, R. G. A. Wills and F. C. Walsh, *Surf. Coat. Technol*., 201 (2006) 371.
32. N. Guglielmi, *J. Electrochem. Soc*., 119 (8) (1972) 1009.
33. Z. Abdel Hamid and S. M. El–Sheikh, *J. Metallurgical Engineering*, 2 (2) (2013) 71.
34. M. Alizadeh, M. Mirak, E. Salahinejad, M. Ghaffari, R. Amini and A. Roosta, *J. Alloys Compd*., 611 (2014) 161.
35. F. Cai and C. Jiang, *Appl. Surf. Sci.,* 292 (2014) 620.
36. B. R. Tian and Y. F. Cheng, *Electrochim. Acta*, 53 (2007) 511.
37. Z. Yue–bo, Z. Guo–gang and Z. Hai–jun, *Trans. of Nonferrous Metals Soc. of China*, 20 (2010) 104.
38. A. Goral, M. Nowak, K. Berent and B. Kania, *J. Alloys Compd*., 615 (1) (2014) S406.
39. B. Bakhit and A Akbari*J. Alloys Compd*., 560 (2013) 92.
40. R. K. Saha and T. I. Khan, *Surf. Coat. Technol*., 205 (2010) 890.
41. D. K. Singh and V. B. Singh, *Mater. Sci. Eng*., A, 532 (2012) 493.
42. P. Baghery, M. Farzam, A. B. Mousavi and M. Hosseini *Surf. Coat. Technol*., 204 (2010) 3804.
43. S. Kasturibai and G. Paruthimal Kalaignan, *Mater. Chem. Phys*., 147 (2014) 1042.
44. M. R. Vaezi, S. K. Sadrnezhaad and L. *Colloids Surf., A Physicochem. Eng. Aspects*, 315 (2008) 176.
45. A. Abdel Aal, K. M. Ibrahim and Z. Abdel Hamid*, Wear*, 260 (2006) 1070.
46. I. Napłoszek–Bilnik, A. Budniok, B. Łosiewicz, L. Pająk and E. Łągiewka, *Thin Solid Films*, 474 (2005) 146.
47. G. N. K. Ramesh Bapu and S. Jayakrishnan, *Surf. Coat. Technol*., 206 (2012) 2330.
48. J. A. Calderón, J. E. Henao and M. A. Gómez, *Electrochim. Acta*, 124 (2014) 1908.
49. F. Kılıç, H. Gül, S. Aslan, A. Alp and H. Akbulut, *Colloids Surf., A: Physicochem. Eng. Aspects*, 419 (2013) 53.
50. M. M. Kamel, Z. M. Anwer, I. T. Abdel–Salam and I. S. Ibrahim, *Surf. Interface Anal*., 46 (2014) 442.
51. M. M. Kamel, *J. Appl. Electrochem*., 37 (2007) 483.
52. B. Bakhit and A. Akbari, *Surf. Coat. Technol*., 253 (2014) 76.
53. Y. H. You, C. D. Gu, X. L. Wang and J. P. Tu, *Surf. Coat. Technol*., 206 (2012) 3632.
54. C. Gheorghies, G. Carac and I. V. Stasi, Journal of Optoelectronics. & Adv. Mate., 8 (3) (2006) 1234.
55. T. Borkar and S. P. Harimkar, *Surf. Coat. Technol*., 205 (2011) 4124.
56. M. Srivastava, V. K. William Grips and K. S. Rajam, *Appl. Surf. Sci.,* 257 (2010) 717.
57. B. M. Praveen and T. V. Venkatesha, *Appl. Surf. Sci.,* 254 (2008) 2418.
58. R. Sen, S. Das and K. Das, *Surf. Coat. Technol*., 205 (2011) 3847.
59. Q. Feng, T. Li, H. Teng, X. Zhang, Y. Zhang, C. Liu and J. Jin, *Surf. Coat. Technol*., 202 (2008) 4137.
60. B. Bahadormanesh, A. Dolati and M. R. Ahmadi, *J. Alloys Compd*, 509 (2011) 9406.
61. S. T. Aruna, C. Anandan and V. K. William Grips, *Appl. Surf. Sci*., 301 (2014) 383.
62. M. Srivastava, J. N. Balaraju, B. Ravishankar and K. S. Rajam, *Surf. Coat. Technol*., 205 (2010) 66.
63. M. A. Shoeib, M. M. Kamel, S. M. Rashwan and O. M. Hafez, *Surf. Interface Anal*., 47 (2015) 672.
64. Y. Xiu–ying, L. Kang–ju, P. Xiao and W. Fu–hui, *Transactions of Nonferrous Metals Society of China,* 19 (2009) 119.

65. Z. Guo–gang, Z. Yue–bo and Z. Hai–jun, *Transactions of Nonferrous Metals Society of China*, 19 (2009) 319.